2023-05-01

Steady decline in mean annual air temperatures in the first 30 k.y. after the Cretaceous-Paleogene boundary

O'Connor, LK

10.1130/g50588.1
Geology
Geological Society of America

Steady decline in mean annual air temperatures in the first 30 ka after the Cretaceous-Paleogene boundary

Lauren K. O'Connor[1]*^, Emily Dearing Crampton-Flood[1]^, Rhodri M. Jerrett[1], Gregory D. Price[2], B. David A. Naafs[3], Richard D. Pancost[3], Paul McCormack[2], Aris Lempotesis-Davies[1], Bart E. van Dongen[1], & Sabine K. Lengger[2,4]

[1]Department of Earth and Environmental Sciences, University of Manchester, Oxford Road, Manchester, M13 9PL, UK

[2]School of Geography, Earth and Environmental Sciences, Plymouth University, Drake Circus, Plymouth, PL4 8AA, UK

[3]School of Chemistry, School of Earth Sciences, Cabot Institute for the Environment, University of Bristol, BS8 1TS Bristol, UK

[4]Sensor Systems Division, Silicon Austria Labs, Villach 9524, Austria

^Joint first-authorship

Correspondence to: lauren.oconnor@manchester.ac.uk

ABSTRACT

The Cretaceous-Paleogene (K-Pg) boundary marks one of the five major mass extinctions of the Phanerozoic. How the climate system responded to a bolide impact and extensive volcanism at this time over different timescales is highly debated. Here we use the distribution of branched tetraether lipids (brGDGT) from fossil peats at two sites in Saskatchewan, Canada (paleolatitude ~55 °N), to generate a high-resolution (millennial) record of mean annual air temperature (MAAT) spanning the last ~4 ka of the Cretaceous and first ~30 ka of the Paleogene. Our study shows that MAATs ranged from 16–29°C, with the highest value in the first millennia of the Paleogene. The earliest Paleogene averaged ~25°C—maintaining or enhancing warmth of the latest Cretaceous,

followed by a general cooling to ~20°C over the following ~30 ka. No abrupt post-boundary cooling (e.g., an "impact winter") or warming are evident in our data, implying that if such phenomena occurred, their duration was relatively short-lived, (i.e., sub-millennial). Further, no long-term impact- or volcanism-driven warming is evident. As such, hypothesized mechanisms of millennial-scale temperature change at the K-Pg boundary must be reassessed in light of our new high-resolution data. The range of temperature change observed is considerably greater than that derived from marine proxy records over the same time interval. Our findings therefore more properly place bounds on the magnitudes and durations of temperature change on land during this interval of time—the main setting in which the demise of the dinosaurs and the rise of mammals occurred.

INTRODUCTION

The Cretaceous-Paleogene (K-Pg) boundary marks one of the five major mass extinctions of the Phanerozoic. Climate change triggered by bolide impact on the Yucatán Peninsula and Deccan Trap volcanism is implicated in the mass extinction, but how different parts of the climate system responded to these triggers and at what timescales remains highly debated (e.g., Schoene et al. 2019; Sprain et al. 2019; Hull et al. 2020). Both the impact and volcanism have spurred numerous models of their effect on climate, but tests of these hypotheses are hampered, in part, by a lack of sufficiently resolved temperature constraints close to the boundary itself, especially from the terrestrial realm.

Bolide impact models suggest an intense heat pulse in the first minutes to hours after impact caused by the return flux of larger ejecta and flash heating of the atmosphere (Lewis et al. 1982; Melosh et al. 1990); an "impact winter" lasting months to millennia, due to atmospheric loading of dust, soot, and sulfate aerosols (Pope, et al. 1994; Bardeen et al. 2017; Brugger et al., 2017); and greenhouse heating caused by CO_2 from impact-volatilized carbonates (and wildfires) beginning 10^3 years after impact (O'Keefe and Ahrens 1989). Establishing a relationship between Deccan volcanism and climate change at the K-Pg boundary is limited by difficulties in dating the lava flows (Schoene et

al. 2019; Sprain et al. 2019) and constraining the amount and rate of associated CO_2 and SO_2 release (Self et al. 2006; Schmidt et al. 2016). Nevertheless, a compilation of global temperature records across the K-Pg boundary (Hull et al. 2020) shows: (1) that an episode of warming (~2°C) between 350 and 200 ka before the K-Pg boundary was coincident with the onset of volcanism; (2) a subsequent decline in temperatures lasting until the boundary itself, likely driven by absorption of CO_2 into the ocean following the cessation of outgassing; and (3) that the first 1 Ma of the Paleocene was characterized by warming of ~1°C. Discrete reconstructions of temperature change at the K-Pg boundary at higher temporal resolution are confined to shallow-marine records (e.g., Vellekoop et al. 2016). Because it is not known whether the atmosphere-ocean climate system was coupled at this time, high-resolution air temperature data are required to develop a holistic understanding of the global response to events at the K-Pg boundary, and to contextualize climate change on land—the main setting for the demise of the dinosaurs and rise of mammals.

In this study, we apply a lipid biomarker paleotemperature proxy (MBT'5Me; Weijers et al. 2007; Naafs et al. 2017) to fossil peats (coals) to reconstruct mean annual air temperatures (MAAT) at a millennial resolution across the K-Pg boundary. The coals are from two sites located 45 km apart—Wood Mountain Creek and Rock Creek West (Saskatchewan, Canada)—which lay at a palaeolatitude of 54–56°N at the time of deposition (van Hinsbergen et al. 2015; Fig. 1).Both coals contain the distinctive Ir-enriched claystone, palynological extinction, and fern-spore spike that globally mark the boundary (Sweet and Braman 1992). The Ir-anomaly claystone and $\delta^{13}C_{org}$ stratigraphies of the coals are used to correlate the two sites and produce a composite MAAT record. These data allow the testing, for the first time, of hypothesized terrestrial climate change at the K-Pg boundary at the timescales of 10^3 to 10^4 years.

APPROACH AND METHODS

The MBT'_{5Me} proxy is based on branched glycerol dialkyl glycerol tetraethers (brGDGTs), which are membrane lipids produced by bacteria. The degree of methylation of these branched tetraethers

(MBT) is dependent on the temperature at which the molecule was metabolized, allowing for their use as a MAAT proxy as far back as the Paleogene (e.g., Naafs et al. 2018).

Coal seams from Wood Mountain Creek (49°25'20"N 106°19'50"W) and Rock Creek West (49°02'20"N 106°34'00"W) were sampled contiguously (Fig. 2), and freeze-dried and powdered for geochemical analysis (Supplementary Material). Samples were solvent extracted using a MARS6 microwave extraction system. The total lipid extracts (Wood Mountain Creek) or polar fractions (Rock Creek West) were dissolved in a hexane-isopropanol mixture (99:1, v/v), filtered (0.45 µm PTFE) using hexane:isopropanol (99:1, v/v), and analyzed using high performance liquid chromatography-atmospheric pressure chemical ionization-mass spectrometry (HPLC/APCI-MS) on a ThermoFisher Scientific Accela Quantum Access triple quadrupole (Wood Mountain Creek, University of Bristol) and a TSQ Quantum Access Orbitrap HPLC-MS (Rock Creek West, University of Plymouth; Vickers et al. 2020). The apolar fractions were then analyzed using an Agilent 5975C gas chromatograph with an Agilent 5975C MSD mass spectrometer. Bulk organic $\delta^{13}C$ analyses were conducted at Plymouth University using an Isoprime mass spectrometer connected to an Isoprime Microcube elemental analyzer.

TEMPERATURE DATA, CORRELATION, AND AGE MODEL

The brGDGT records from both sites show similar absolute values, translating to MAATs (Naafs et al. 2017) ranging from 16.7–27.9 ± 4.7°C at Rock Creek West and 14.4–29.1 ± 4.7°C at Wood Mountain Creek (Fig. S2). The similarity in the two records, in both absolute values and trends, provides confidence in the fidelity of the individual records. $\delta^{13}C$ values at both sites are similar (-25.5 to -21.1 ‰ at Rock Creek West and -27.2 to -21.9 ‰ at Wood Mountain Creek), and show recognizable excursions with similar shapes and magnitudes that allow for reliable correlation between the sites (Fig. 2). The Ir-enriched claystone is used as the primary datum for correlation between the two sites. The inflexion points on the $\delta^{13}C$ curves are used as secondary, independent, tie points to produce the composite temperature record (Fig. 3).

Notwithstanding likely differences in rates of peat accumulation and/or compaction between the two sites, it is possible to place bounds on the duration of time represented by the composite record. Absolute age determinations of two tuffs by Renne et al. (2013) at a contemporaneous coal-bearing K-Pg site (Hell Creek Marina Road, Montana), located 170 km SSW of Rock Creek West (Fig. 1), yield for 1 m of coal a most likely duration of ~40 ka (with a maximum duration of up to 175 ka, and an unlikely minimum duration that equates to instantaneous deposition; Supplementary Material). However, modelling of the timing of bolide impact debris fall-out (Goderis et al., 2021), and estimates of the duration of time represented by the fern-spore spike (Clyde et al. 2016) contained within the Ir-enriched impact claystone (Sweet and Braman 1992), imply that the first MAAT datapoint above it must represent at least ~1 ka after bolide impact at the K-Pg boundary (Fig. 3). We use the value for the most likely duration (1 m of coal = 40 ka) to estimate time at our two sites, but continue to acknowledge the uncertainty outlined above (Fig. 3).

Given the difficulty in constraining age in such a high-resolution section, and the large paleotemperature calibration error, we treat detail in our MAAT record cautiously: we focus on the most pronounced trends and have binned the data into 10-ka intervals. Our combined record (Fig. 3) shows general warmth in the latest Cretaceous, albeit with scatter (avg. = 24.5°C ±2.7, n = 7), which increased to the highest MAATs (avg. = 25.2°C ±2.0, n = 21) in the first 10 ka after the K-Pg boundary ($p = 0.13$). The subsequent 10 ka interval experienced a general decline in temperatures (avg. = 22.8°C ±1.8, n = 22, $p = 0.00$), followed by a continued decline to 20.4°C (±2.7, n = 19, $p = 0.00$) over the remaining 10 ka of our record.

DISCUSSION

The absolute MAATs (17–29°C) and binned averages (20-25°C) are more than 10°C higher than modern MAATs at the equivalent latitude in the western interior of North America. However, these data agree with general circulation models (e.g., Sellwood and Valdes 2006; Tabor et al. 2016) and other terrestrial proxy data (Zhang et al. 2019) that indicate temperatures of 20°C in the Arctic to 30°C

at the southern margin of the North American western interior during the K-Pg. These new data support hypotheses of a reduced latitudinal temperature gradients at this time (Zhang et al. 2019).

Several observations stand out from the Saskatchewan record. Firstly, neither abrupt warming nor cooling are observed immediately post-impact. Latest Cretaceous warmth was weakly enhanced by 0.7°C between the last ~4 ka of the Cretaceous and first ~10 ka of the Paleogene (Fig. 3). Climate models suggest that the impact winter lasted only years to decades (Pope et al. 1994; Tabor et al. 2016; Bardeen et al. 2017), which is below the resolution of our record. Our data therefore do not preclude an episode of post-impact cooling at the timescales indicated by these models. However, our data do not support the notion of an impact winter lasting more than a thousand years, as interpreted from the shallow-marine record of Vellekoop et al. (2014). The "winter" observed in this record occurs within the interpreted fall-out of the waning tail of a tsunami, which, irrespective of linear time-interpolation models, represents a geologically instantaneous event bed. Further, the origin of organic matter within such deposits should also be treated with caution, given the potential of such flows to entrain and transport sediment from marine and terrestrial environments.

There is no evidence for abrupt global warming and sustained over10^4–10^5 years as suggested by some models (O'Keefe and Ahrens 1989), and purportedly supported by marine (e.g., MacLeod et al. 2018; Taylor et al. 2018) and terrestrial (Lyson et al. 2019) proxy data. Though the highest individual MAAT datapoints of our record occur in within the first 10 ka of the Paleogene, our data suggest this interval was preceded by general warming in the last 5 ka of the Cretaceous (Fig. 3). This trend is also evident in the relatively high-resolution benthic marine record of Barnet et al. 2017). The "abrupt" 3–5°C of warming in existing records (MacLeod et al. 2018; Taylor et al. 2018; Lyson et al. 2019) may be an artifact of low-resolution spot-sampling. In those studies, a there is a temporal gap of no less than ~3 ka before the last Cretaceous datapoint and the K-Pg boundary itself. The data from these studies are consistent with our results, insofar as there is a temperature increase across the K-Pg boundary, but we posit that these values represent the culmination of a longer-term warming trend—pre-dating the bolide impact—and cannot be considered "abrupt". Although bolide impact is inextricably linked

157 to the mass extinction, its effect on terrestrial temperatures appears to have been modest at most;
158 either weakly enhancing an already existing latest Cretaceous warmth or failing to interrupt pre-
159 existing trend of latest Cretaceous warming.

160 Early Paleogene warmth cannot be said to be "sustained" at the timescales implied by models
161 of global warming caused by impact-volatilization (O'Keefe and Ahrens, 1989) in our data. Irrespective
162 of the most likely (30 ka) or longest possible (130 ka) duration for our earliest Paleogene record, we
163 document a steady decline in MAAT in the tens of thousands of years that follow the K-Pg boundary,
164 most likely driven by the sequestration of carbon by biomass recovery in the wake of the mass
165 extinction (e.g., Lyson et al. 2019). The marine $\delta^{18}O$ records of Barnet et al. (2019) from the South
166 Atlantic and MacLeod et al. (2018) from the Tethyan K-Pg type section at El Kef (Tunisia) document 1-
167 2°C of cooling over ~30 Ka, and up to 5°C of cooling over up to 200 ka respectively. The timescales of
168 cooling in these studies are within the error margin of the this study and one-another. From the
169 terrestrial realm, lower-resolution qualitative palaeobotanical studies from the western interior of
170 North America that indicate lower temperature relative to the latest Cretaceous mean within the first
171 ~100 ka of the Paleogene (Davies-Vollum and Wing 1998; Wilf et al. 2003; Peppe 2010; Lyson, et al.
172 2019). Overall, data converge on the notion of temperature maxima immediately following the K-Pg
173 boundary, followed by several tens of thousands of years, at least, of cooling in the earliest Paleogene.
174 Mechanistically, MAAT decline over these timescales were most likely driven by the sequestration of
175 carbon linked to the rapid recovery of biomass at this time (e.g. Lyson et al., 2019), irrespective of the
176 source (bolide impact-associated volatilization and wildfires or Deccan volcanism) of CO_2.

177 Finally, relative to comparable marine records, the magnitude (up to 5°C in the binned data)
178 of MAAT change in our data is greater than that of Barnet et al. (2017), but similar to that of MacLeod
179 et al. (2018). Owing to the different thermal masses of land and ocean, differences in the magnitude
180 and duration of temperature change in response to external drivers might be expected (Sutton et al.
181 2007). Understanding and quantifying these differences is limited by the error margins of age models
182 and temporal resolution of existing data. As such, the generation of directly comparable, time-

calibrated marine and terrestrial archives is critical to a holistic understanding of the entire ocean-atmosphere system.

CONCLUSION

We observe similar absolute values and trends of terrestrial temperature change across the K-Pg boundary at two closely spaced fossil peats that were located at ~55°N in what is now southern Saskatchewan. This similarity has permitted the generation of a millennial-scale, composite MAAT record through this critical time interval. MAATs peaked at ~25°C within the first ~10 ka of the Paleogene, which we tentatively interpret to represent the weak enhancement of warmth from the last ~4 ka of the Cretaceous. Peak warmth was followed by ~5°C cooling over the following 20 ka, most likely driven by the sequestration of carbon by biomass recovery in the wake of the mass extinction. We observe no abrupt "impact winter" nor a spike in temperature immediately following the boundary. If such phenomena occurred, their duration was below the resolution of our record: ~1 ka. Our data highlight the value of peat as a sensitive, high-resolution palaeotemperature archive, and place new bounds on the magnitude and rate of millennial-scale MAAT change in the terrestrial realm—the main setting for the demise of the dinosaurs and the rise of mammals.

ACKNOWLEDGEMENTS

The study was funded by UK Natural Environment Research Council grant NE/S002324/1 awarded to RMJ. BDAN also acknowledges funding through a Royal Society Tata University Research Fellowship. Thanks to Grasslands National Park for allowing access to Rock Creek West, and Ritchie Hordenchuk for access to Wood Mountain Creek. Thanks to Steve Stockley, Abby Ragazzon-Smith, and Paul Lythgoe (University of Manchester), Marc Davies and Steve Rowland (University of Plymouth), and Ian Bull (University of Bristol) for technical assistance.

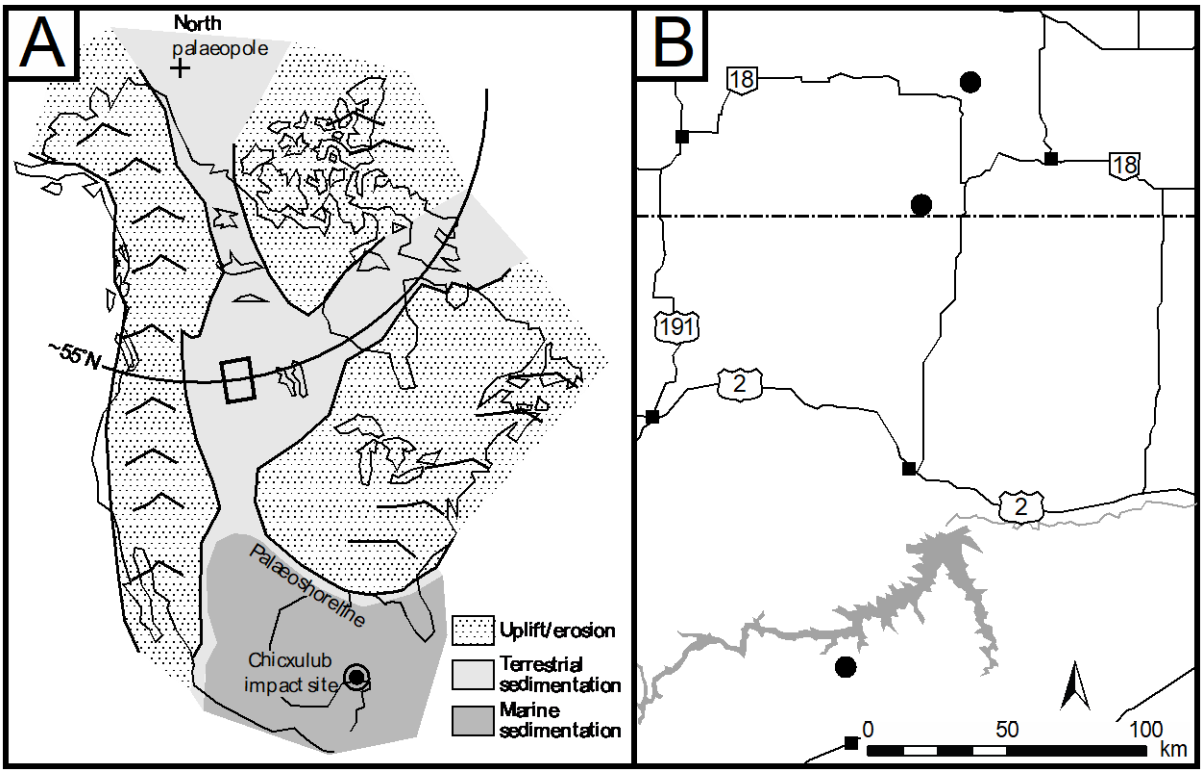

208

209 ***Figure 1.*** *[A] Cretaceous-Paleogene paleogeography of North America (based on Smith et al. 1981 and*

210 *van Hinsbergen et al. 2015) and study area in [B] outlined by black box. [B] Inset of study area with*

211 *modern geography showing the locations of sites named in this study. We use samples from Wood*

212 *Mountain Creek and Rock Creek West.*

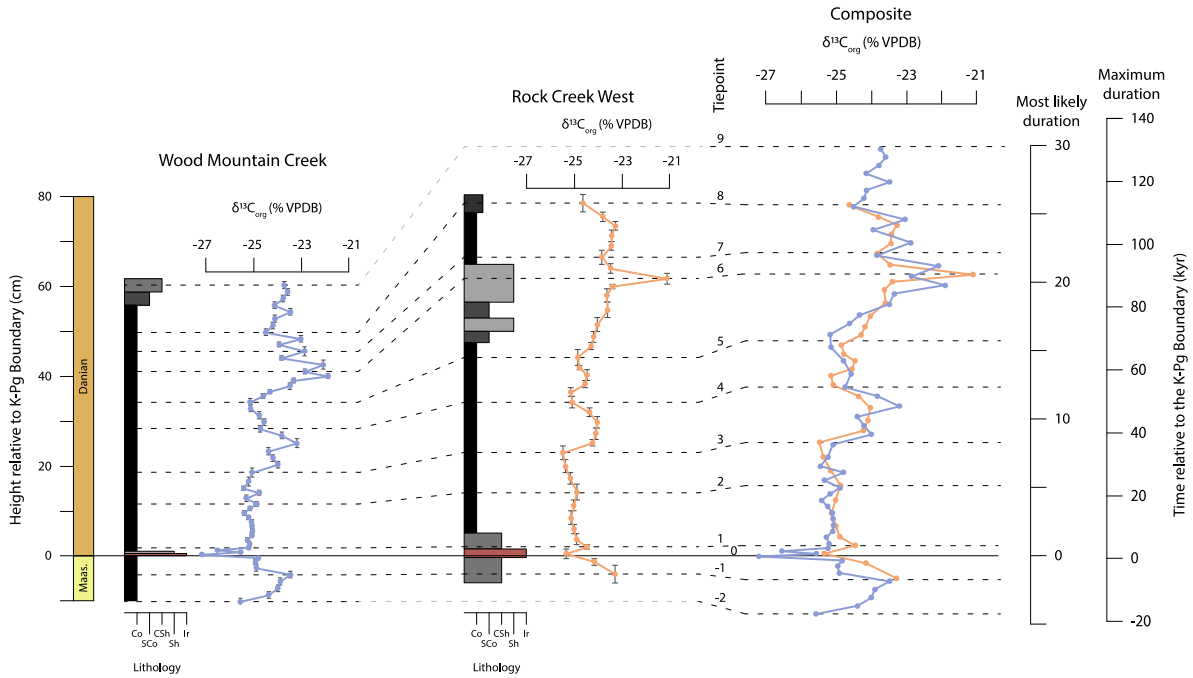

213

Figure 2. *$\delta^{13}C_{org}$ records from Wood Mountain Creek (blue) and Rock Creek West (orange), Saskatchewan. plotted against height above the K-Pg boundary. Vertical error bars show the stratigraphic range of each sample. Dashed lines show chemostratigraphic ($\delta^{13}C$) correlation tiepoints, numbered 1–9 (Supplementary Table S3). Solid line shows the Ir-claystone K-Pg datum. The composite record is plotted against time, with the most likely (40 ka/m of coal) and maximum (175 ka/m of coal) durations shown. On the lithology log, Co = coal, ShC = shaley coal, CSh = coaly shale, Sh = shale, and Ir = iridium-enriched claystone.*

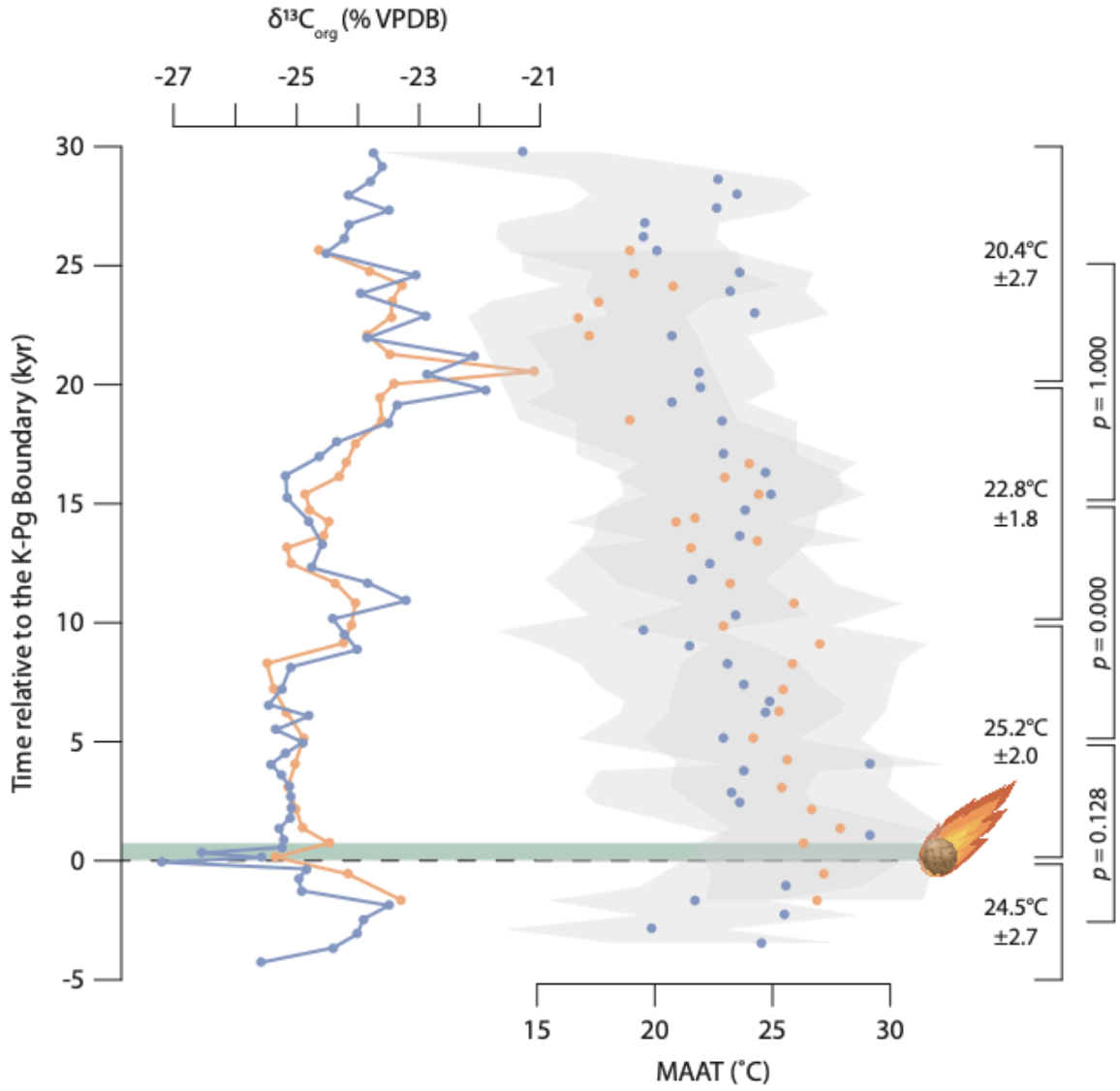

Figure 3. *Composite $\delta^{13}C_{org}$ and mean annual air temperature (MAAT) records from Wood Mountain Creek blue) and Rock Creek West (orange) plotted against time relative to the K-Pg boundary (using*

the most likely duration). The dashed line represents the K-Pg boundary. Average MAATs ± 1 standard deviation for each temporal bin are shown to the right with P values of t tests comparing means (Table S5). The green box must represent at least ~1 ka after bolide impact at the K-Pg boundary.

REFERENCES

Bardeen, C. G., Garcia, R. R., Toon, O. B., & Conley, A. J., 2017, On transient climate change at the Cretaceous−Paleogene boundary due to atmospheric soot injections: Proceedings of the National Academy of Sciences, 114(36), E7415-E7424, doi: 10.1073/pnas.1708980114

Barnet, J. S., Littler, K., Westerhold, T., Kroon, D., Leng, M. J., Leng, M.J., Bailey, I., Röhl, U. & Zachos, J.C., 2017, A high-Fidelity benthic stable isotope record of late Cretaceous–early Eocene climate change and carbon-cycling: Paleoceanography and Paleoclimatology, 34(4), 672-691, doi: 10.1029/2019pa003556

Brugger, J., Feulner, G., & Petri, S., 2017, Baby, it's cold outside: Climate model simulations of the effects of the asteroid impact at the end of the Cretaceous: Geophysical Research Letters, 44(1), 419-427, doi: 10.1002/2016gl072241

Clyde, W. C., Ramezani, J., Johnson, K. R., Bowring, S. A., & Jones, M. M. (2016). Direct high-precision U–Pb geochronology of the end-Cretaceous extinction and calibration of Paleocene astronomical timescales. Earth and Planetary Science Letters, 452, 272-280, doi:10.1016/j.epsl.2016.07.041

Davies-Vollum, K. S. & Wing, S. L., 1998, Sedimentological, taphonomic, and climatic aspects of Eocene swamp deposits (Willwood Formation, Bighorn Basin, Wyoming): Palaios 13, 28-40, doi:10.2307/3515279

De Jonge, C., Hopmans, E. C., Zell, C. I., Kim, J. H., Schouten, S., & Damsté, J. S. S., 2014, Occurrence and abundance of 6-methyl branched glycerol dialkyl glycerol tetraethers in soils: Implications

for palaeoclimate reconstruction: Geochimica et Cosmochimica Acta, 141, 97-112, doi:10.1016/j.gca.2014.06.013

Gooderis, S., Sato, H., Ferriere, L., Schmidt, B., Burney, D., Kaskes, P., Vellekoop, J., Wittmann, A., Schulz, T., et al., 2021, Globally distributed iridium layer preserved within the Chizculub impact structure: Science Advances, 7, eabe3647. doi:10.1126/sciadv.abe3647

Hull, P. M., Bornemann, A., Penman, D. E., Henehan, M. J., Norris, R. D., Wilson, P. A., Blum, P., Alegret, L., Batenburg, S.J., Bown, P.R. and Bralower, T.J., et al., 2020, On impact and volcanism across the Cretaceous-Paleogene boundary: Science, 367(6475), 266-272, doi:10.1126/science.aay5055

Inglis, G. N., Farnsworth, A., Collinson, M. E., Carmichael, M. J., Naafs, B. D. A., Lunt, D. J., Valdes, P.J. & Pancost, R.D., 2019, Terrestrial environmental change across the onset of the PETM and the associated impact on biomarker proxies: A cautionary tale: Global and Planetary Change, 181, 102991, doi:10.1016/j.gloplacha.2019.102991

Lewis, J., Watkins, H., Hartman H., & Prinn, R., 1982, Chemical consequences of major impacts on Earth: Geological Society of America Special Paper 190, 1982. 215-221, doi:10.1130/spe190-p215

Lyson, T. R., Miller, I. M., Bercovici, A. D., Weissenburger, K., Fuentes, A. J., Clyde, W. C., Hagadorn, J.W., Butrim, M.J., Johnson, K.R., Fleming, R.F., et al., 2019, Exceptional continental record of biotic recovery after the Cretaceous–Paleogene mass extinction. Science, 366(6468), 977-983, doi:10.1126/science.aay2268

MacLeod, K. G., Quinton, P. C., Sepúlveda, J., & Negra, M. H., 2018, Postimpact earliest Paleogene warming shown by fish debris oxygen isotopes (El Kef, Tunisia): Science, 360(6396), 1467-1469, doi:10.1126/science.aap8525

271 Melosh, H. J., Schneider, N. M., Zahnle, K. J., & Latham, D., 1990, Ignition of global wildfires at the
272 Cretaceous/Tertiary boundary: Nature, 343(6255), 251-254, doi:10.1038/343251a0

273 Naafs, B.D.A., Inglis, G.N., Zheng, Y., Amesbury, M.J., Biester, H., Bindler, R., Blewett, J., Burrows, M.A.,
274 Del Castillo Torres, D., Chambers, F.M., et al., 2017, Introducing global peat-specific
275 temperature and pH calibrations based on brGDGT bacterial lipids: Geochimica et
276 Cosmochimica Acta, 208, 285-301, doi:10.1016/j.gca.2017.01.038

277 Naafs, B. D. A., Rohrssen, M., Inglis, G. N., Lähteenoja, O., Feakins, S. J., Collinson, M. E., Kennedy, E.M.,
278 Singh, P.K., Singh, M.P., Lunt, D.J., et al., 2018, High temperatures in the terrestrial mid-latitudes
279 during the early Palaeogene: Nature Geoscience, 11(10), 766-771, doi: 10.1038/s41561-018-
280 0199-0

281 O'Keefe, J. D., & Ahrens, T. J., 1989, Impact production of CO2 by the Cretaceous/Tertiary extinction
282 bolide and the resultant heating of the Earth: Nature, 338(6212), 247-249,
283 doi:10.1038/338247a0

284 Peppe, D. J., 2010, Megafloral change in the early and middle Paleocene in the Williston Basin, North
285 Dakota, USA: Palaeogeography, Palaeoclimatology, Palaeoecology 298, 224-234,
286 doi:10.1016/j.palaeo.2010.09.027

287 Pope, K. O., Baines, K. H., Ocampo, A. C., & Ivanov, B. A., 1994, Impact winter and the
288 Cretaceous/Tertiary extinctions: Results of a Chicxulub asteroid impact model: Earth and
289 Planetary Science Letters, 128(3-4), 719-725, doi:10.1016/0012-821X(94)90186-4

290 Renne, P. R., Deino, A. L., Hilgen, F. J., Kuiper, K. F., Mark, D. F., Mitchell III, W. S., Morgan, L.E., Mundil,
291 R. & Smit, J., 2013, Time scales of critical events around the Cretaceous-Paleogene boundary:
292 Science, 339(6120), 684-687, doi:10.1126/science.1230492

293 Schmidt, A., Skeffington, R. A., Thordarson, T., Self, S., Forster, P. M., Rap, A., Ridgwell, A., Fowler, D.,
294 Wilson, M., Mann, G.W., et al., 2016, Selective environmental stress from sulphur emitted by
295 continental flood basalt eruptions. Nature Geoscience, 9(1), 77-82, doi:10.1038/ngeo2588

296 Schoene, B., Eddy, M. P., Samperton, K. M., Keller, C. B., Keller, G., Adatte, T., & Khadri, S. F., 2019, U-
297 Pb constraints on pulsed eruption of the Deccan Traps across the end-Cretaceous mass
298 extinction: Science, 363(6429), 862-866, doi:10.1126/science.aau242

299 Self, S., Widdowson, M., Thordarson, T., & Jay, A. E., 2006, Volatile fluxes during flood basalt eruptions
300 and potential effects on the global environment: A Deccan perspective: Earth and Planetary
301 Science Letters, 248(1-2), 518-532, doi:10.1016/j.epsl.2006.05.041

302 Sellwood, B. W., & Valdes, P. J., 2006, Mesozoic climates: General circulation models and the rock
303 record: Sedimentary geology, 190(1-4), 269-287, doi:10.1016/j.sedgeo.2006.05.013

304 Smith, A. G., Hurley, A. M., & Briden, J. C. (1981). Phanerozoic paleocontinental world maps (Vol. 102).
305 Cambridge: Cambridge University Press

306 Sprain, C. J., Renne, P. R., Vanderkluysen, L., Pande, K., Self, S., & Mittal, T., 2019, The eruptive tempo
307 of Deccan volcanism in relation to the Cretaceous-Paleogene boundary: Science, 363(6429),
308 866-870, doi:10.1126/science.aav1446

309 Sutton, R. T., Dong, B., & Gregory, J. M., 2007, Land/sea warming ratio in response to climate change:
310 IPCC AR4 model results and comparison with observations: Geophysical research letters, 34(2),
311 doi:10.1029/2006gl028164

312 Sweet, A. R., & Braman, D. R., 1992, The KT boundary and contiguous strata in western Canada:
313 interactions between paleoenvironments and palynological assemblages: Cretaceous Research,
314 13(1), 31-79, doi:10.1016/0195-6671(92)90027-N

315 Tabor, C. R., Poulsen, C. J., Lunt, D. J., Rosenbloom, N. A., Otto-Bliesner, B. L., Markwick, P. J., Brady,
316 E.C., Farnsworth, A., & Feng, R., 2016, The cause of Late Cretaceous cooling: A multimodel-proxy
317 comparison: Geology, 44(11), 963-966, doi:10.1130/G38363.1

318 Taylor, K. W., Willumsen, P. S., Hollis, C. J., & Pancost, R. D., 2018, South Pacific evidence for the long-
319 term climate impact of the Cretaceous/Paleogene boundary event: Earth-Science Reviews, 179,
320 287-302, doi:10.1016/j.earscirev.2018.02.012

321 van Hinsbergen, D. J., De Groot, L. V., van Schaik, S. J., Spakman, W., Bijl, P. K., Sluijs, A., Langereis,
322 C.G., & Brinkhuis, H., 2015, A paleolatitude calculator for paleoclimate studies: PloS one, 10(6),
323 e0126946, doi:10.1371/journal.pone.0126946

324 Vellekoop, J., Esmeray-Senlet, S., Miller, K. G., Browning, J. V., Sluijs, A., van de Schootbrugge, B.,
325 Damsté, J.S.S., & Brinkhuis, H., 2016, Evidence for Cretaceous-Paleogene boundary bolide
326 "impact winter" conditions from New Jersey, USA: Geology, 44(8), 619-622,
327 doi:10.1130/G37961.1

328 Vellekoop, J., Sluijs, A., Smit, J., Schouten, S., Weijers, J. W., Sinninghe Damsté, J. S., & Brinkhuis, H.,
329 2014, Rapid short-term cooling following the Chicxulub impact at the Cretaceous–Paleogene
330 boundary: Proceedings of the National Academy of Sciences, 111(21), 7537-7541,
331 doi:10.1073/pnas.1319253111

332 Vickers, M. L., Lengger, S. K., Bernasconi, S. M., Thibault, N., Schultz, B. P., Fernandez, A., Ullmann,
333 C.V., McCormack, P., Bjerrum, C.J., Rasmussen, J.A., et al., 2020, Cold spells in the Nordic Seas
334 during the early Eocene Greenhouse: Nature communications, 11(1), 1-12, doi:0.1038/s41467-
335 020-18558-7

336 Weijers, J. W., Schouten, S., van den Donker, J. C., Hopmans, E. C., & Damsté, J. S. S., 2007,
337 Environmental controls on bacterial tetraether membrane lipid distribution in soils: Geochimica
338 et Cosmochimica Acta, 71(3), 703-713, doi:10.1016/j.gca.2006.10.003

Wilf, P., Johnson, K. R. & Huber, B. T. (2003) Correlated terrestrial and marine evidence for global climate changes before mass extinction at the Cretaceous–Paleogene boundary. Proceedings of the National Academy of Sciences 100, 599-604.

Zhang, L., Hay, W. W., Wang, C., & Gu, X., 2019, The evolution of latitudinal temperature gradients from the latest Cretaceous through the Present: Earth-Science Reviews, 189, 147-158, doi:10.1016/j.earscirev.2019.01.025

SUPPLEMENTARY MATERIAL

Site description and sampling

The Ferris Coal at Wood Mountain Creek (49°25′20″N 106°19′50″W) and Rock Creek West (49°02′20″N 106°34′00″) has been shown to span the K-Pg boundary, based on the distinctive 1–2 cm thick pink- to buff-coloured Ir-enriched claystone contained in each section (Nichols et al. 1986; Sweet and Braman 1992). The claystone is also coincident with a palynologically defined extinction of Cretaceous flora (Sweet and Braman 1992). At the time of the K-Pg boundary, the sites were (1) peat mires accumulating in the foreland basin of the ancestral Rocky Mountains; (2) inland, approximately equidistant between the shorelines of the (proto) Gulf of Mexico and the Boreal Sea (now the Arctic Ocean; Fig. 1); (3) at a palaeolatitude of approximately 54–56°N (van Hinsbergen et al. 2015); and (4) at negligible altitude, as evidenced by the persistence of marine conditions in the Maastrichtian Bearpaw Formation some tens of metres below the K-Pg boundary (Sweet and Braman, 2001). Vitrinite reflectance data (R_o) values for the Ferris Coal at the sites are <0.38%, indicating lignite rank (Bustin 1991).

At both sites, the entire coal seam was contiguously sampled. Wood Mountain Creek was sampled in 2011 (56 samples). Sampling methodology and $\delta^{13}C_{org}$ analyses were previously published in Jerrett et al. (2015) and the latter are re-reported in Supplementary Table S1. Remaining material from the Wood Mountain Creek site were used for brGDGT analysis in this study. Rock Creek West was sampled in 2019 (36 samples), using the method described in Jerrett et al. (2015).

Geochemical analysis and brGDGT method validation

All samples were freeze-dried and finely ground using a granite pestle and mortar prior to geochemical analyses.

Wood Mountain Creek

Approximately 0.5 g of sediment was solvent-extracted using ~20mL of DCM/methanol (9:1, v/v) in a Milestone Ethos Ex microwave extraction system at the Organic Geochemistry Unit (OGU) at the University of Bristol. Temperature in the microwave was programmed to increase linearly from room temperature to 70°C over 10 min at which it was held for 10 min, and then cooled to 25°C over 20 minutes. The total lipid extract (TLE) was dissolved in hexane:propanol (99:1, v/v) and filtered (0.45 µm PTFE) prior to analysis.

Samples were analysed for their GDGT content by high-performance liquid chromatography/atmospheric pressure chemical ionization–mass spectrometry (HPLC/APCI-MS) at the University of Bristol using a ThermoFisher Scientific Accela Quantum Access. Normal-phase separation was achieved using an Alltech Prevail Cyano column (150 mm x 2.1 mm; 3 µm internal diameter). Isocratic elution for 5 min using hexane:isopropanol 99:1 (v/v) was followed by a linear gradient to 1.8% isopropanol (45 min). Selective ion monitoring (SIM) was used to detect the $[M+H]^+$ ions of the following masses: *m/z* 1050, 1048, 1046, 1036, 1034, 1032, 1022, 1020, 1018, 744). The average standard deviation for duplicate MBT' measurements of an in-house standard was 0.026 units. The data are reported in Supplementary Table S1. The MBT'5Me index was calculated following De Jonge et al. (2014):

$$\mathrm{MBT'5Me} = \frac{[\mathrm{Ia}] + [\mathrm{Ib}] + [\mathrm{Ic}]}{[\mathrm{Ia}] + [\mathrm{Ib}] + [\mathrm{Ic}] + [\mathrm{IIa}] + [\mathrm{IIb}] + [\mathrm{IIc}] + [\mathrm{IIIa}]}$$

The peat specific calibration ($MAAT_{peat}$, Naafs et al. 2017) was used to convert MBT'5Me values into mean annual air temperatures:

$$\mathrm{MAAT_{peat}}\ (°\mathrm{C}) = 52.18(\mathrm{MBT'5Me}) - 23.05$$

Rock Creek West

For $\delta^{13}C_{org}$ analysis, samples were oven dried (30°C, 24 h), and decarbonated using hydrochloric acid (10% v/v) until any visible reaction had ceased. The samples were then repeatedly washed with

deionised water until a neutral solution was obtained, and oven dried again (30°C, 24 h). Carbon isotope analyses were conducted at the University of Plymouth using a Thermo Scientific Delta V Advantage. Carbon-isotope ratios are expressed using the internationally accepted per mil (‰) standard notation relative to the Vienna Peedee belemnite (VPDB) standard (Supplementary Table S1). Instrument calibration was achieved using three international standards: USGS 40 (l-glutamic acid, $\delta^{13}C$ = -26.389‰), USGS 24 (graphite, $\delta^{13}C$ = -16.049‰), and IAEA CH-7 (polyethylene, $\delta^{13}C$ = -32.151‰). The standard deviation on replicates in run analyses of the USGS 40 standard was ±0.12‰.

Approximately 1 g of sediment was solvent-extracted using 20mL of DCM/methanol (9:1, v/v) in a microwave assisted reactor system (MARS 6, CEM) at the University of Manchester following the same protocol as for Wood Mountain Creek. The TLE was separated into polar and apolar fractions by column chromatography, using hexane/DCM (9:1, v/v) and DCM/methanol (1:1, v/v) respectively as the eluents, and Al_2O_3 as the stationary phase. The polar fraction was re-dissolved in hexane/propanol (99:1, v/v) and filtered using a 0.45 µm PTFE filter prior to analysis.

Analysis of GDGTs was carried out using a Dionex LPG-U3400(SDN) UHPLC liquid chromatography system and Thermo Scientific Q Exactive Focus mass spectrometer with Atmospheric Pressure Chemical Ionisation (APCI). For the determination of MBT'5Me, the method of Hopmans et al. (2016) was adapted to this high-performance instrument employing a single Waters Acquity UPLC, BEH HILIC 1.7 µm (150 x 2.1 mm, 1.7 µm) column and precolumn at 40°C. Using solvents A (hexane) and B (9:1 hexane:isopropanol v/v) and a flow of 600 µl min -1, the mix started at 5% B (isocratic from 0–3 min), rising to 18 % B at 5 min (isocratic 5–10 min), rising to 35% B at 15 min and 100% B at 17.4 min, with 2.6 min re-equilibration time, which slightly shortened the analysis time. APCI was carried out in positive polarisation mode, at a capillary temperature of 275°C. Masses were scanned from *m/z* 200 to 2000, and resolved to 70,000 at *m/z* 200, with mass calibration carried out externally in electro spray ionisation mode, using auto-calibration Pierce LTQ Velos ESI positive ion calibration solution (n-butylamine, caffeine, MRFA, and Ultramark 1621). GDGTs were identified based on retention times and accurate masses: using 1022.00967 (brGDGT-Ia), 1019.99402 (brGDGT-Ib), 1017.97837 (brGDGT-

Ic), 1036.02532 (brGDGT-IIa+IIa'), 1034.00967 (brGDGT-IIb+IIb'), 1031.99402 (brGDGT-IIc+IIc'), 1050.04097 (brGDGT-IIIa+IIIa'), 1048.02532 (brGDGT-IIIb+IIIb'), 1046.00967 (brGDGT-IIIc+IIIc'), and 1292.24442 (crenarchaeol). Integration was carried out using Xcalibur 4.2 using QuanBrowser integration and data management. The data are reported in Supplementary Table S1.

Comparison of HPLC data from University of Bristol and Plymouth University

To allow comparability between the samples analysed at the University of Bristol and the University of Plymouth, in particular for 6-me separation, a set of standards and unrelated, representative samples, were analyzed at Bristol and Plymouth (marine standard and EH-8, Lengger et al. 2018). Further, as the HPLC-APCI-MS method for GDGT analyses was shortened to allow higher sample-throughput, taking advantage of the UHPLC-Orbitrap-MS system at the University of Plymouth, a subset of standards and samples were run on both methods ('long' for standard method acc. to Hopmans et al. (2016), 'short' method for 20 min method: shown are marine standard and EH-8 as described in Lengger et al. (2018); RCW-26 this work), to determine reproducibility (Supplementary Fig. S1). The 'short' method is a variation of Hopmans et al. (2016), modified to run on one HPLC column (not two), and completes a sample run in 20 minutes (described in Vickers et al. 2020). As a result, the resolution is slightly compromised when compared to Hopmans et al. (2016), though the resolution of the 'short' method is comparable to the method at the University of Bristol (Supplementary Fig. S1). The results from both 'short' and 'long' methods are very similar, with similar MBT' and MBT'5Me values calculated for both (Supplementary Table S2). In addition, the 'long' method was also implemented at Plymouth and used for cross-calibration.

Fidelity of the MAAT record

Where possible, all GDGT analyses were duplicated (Supplementary Table S1). A minority either could not be analysed a second time or showed a standard deviation >1 so were eliminated from the study

447 (Supplementary Table S1). Shale samples were also excluded as the proxy is not meant for non-coals.
448 To explore the fidelity of our GDGT-reconstructed temperatures, we examined the distributions of
449 other GDGTs and biomarkers indicative of depositional environment. Previous work has shown that
450 major changes in depositional setting, as inferred from reconstructed pH, can bias temperature
451 estimates (Weijers et al. 2011; Inglis et al. 2019). The CBT_{peat} index was calculated following De Jonge
452 et al. (2014):

453 $$\mathrm{CBT'} = \log\frac{Ic + IIa' + IIb' + IIc' + IIIa' + IIIb' + IIIc'}{Ia + IIa + IIIa}$$

454 The peat specific calibration (CBT_{peat}, Naafs et al. 2017) was used to convert CBT'5 values into pH:

455 $$\mathrm{pH} = 2.29\left(\mathrm{CBT_{peat}}\right) + 8.07$$

456 In these sections, CBT_{peat}-pH does vary (from 4.4 to 6.8; Supplementary Table S1), though at
457 neither Rock Creek West nor Wood Mountain Creek do these changes correlate with temperature
458 changes. At Rock Creek West there is a decline in pH from 7 to 6.5 from the basal (Cretaceous) parts
459 to the lowermost (Paleogene) parts of the coals, and thereafter vacillates between 5 and 6. At Wood
460 Mountain Creek, the pH is highly variable in the Cretaceous (from 4.4 to 6.3), but in the earliest
461 Paleogene declines from 6.5, and thereafter varies between 5 and 6. The patterns are consistent with
462 palynological (Sweet and Braman 1992) and petrographic (Sweet and Cameron 1991; Jerrett et al.
463 2015) data, that imply that the coal at both sites represents a hydroseral succession upwards from
464 (typically more alkaline) ponded, disconnected forested rheotrophic mires in-filling topographic
465 hollows, to (typically more acidic) aerially expansive herbaceous, possibly ombrotrophic mires.
466 However, we observe no correlation between pH and temperature, and no change in CBT associated
467 with the post-boundary cooling. Although the variations in CBT-derived pH are larger than those
468 observed in other settings (e.g., Lauretano et al. 2021), they are smaller than the previous studies
469 where pH was inferred to bias temperature estimates (Weijers et al. 2011; Inglis et al. 2019). Some of
470 the smaller variations in pH do coincide with changes in reconstructed temperature, so we focus on
471 the main trends in MAAT.

To further explore the wider biomarker deposition at these sites, we determined the bacterial hopane isomerisation ratio; isomerisation at the C_{17} and C_{21} positions (from the 17β,21β(H) to the 17α,21β(H) configuration) normally increases with thermal maturity, but this process is accelerated, especially for the C_{31} hopane, under acidic conditions in wetlands, hence it is not a useful maturity indicator under such conditions (Inglis et al. 2019).

The apolar fractions were analysed using an Agilent 7890A gas chromatograph (GC) interfaced to an Agilent 5975C MSD mass spectrometer (MS) operated in electron ionisation scan/SIM mode (scanning range, *m/z* 50–600; SIM masses used: *m/z* 57, 66, 191 and 205; ionisation energy, 70 eV; solvent delay of 2.5 min) using helium as the carrier gas at a constant flow (1 mL/min). The GC was equipped with an Agilent 7683B auto-sampler and programmable temperature vaporization (PTV) inlet. The samples were dissolved in hexane prior to injection, injected using pulsed split-less injection (1 µL; inlet pressure of 25 psi for 0.75 min), and separated on a Zebron ZB-5MS capillary column (Phenomenex; length 30 m; 250 µm ID, 0.25 µm film thickness). The heated interface (MSD transfer line) and PTV temperatures were set to 280°C, the mass source, at 230°C and the mass spectrometer quadrupole at 150°C. The samples were injected at 50°C and the oven was programmed to ramp to 130°C at 20°C/min and then to 310 °C at 6 °C/min, at which it was kept isothermally for 15 min. Compounds were identified by comparison of their molecular mass (*m/z*) with The National Institute of Standards and Technology (NIST) library. Quantitative data were determined by comparison of individual peak areas with a known concentration of the internal standard deuterated tetracosane, added prior to analyse and pH was calculated using the C_{31} hopanes following Inglis et al. (2018) :

$$\mathrm{pH} = 5.22 \left(\frac{\beta\beta}{\alpha\beta + \beta\beta} \right) + 3.11$$

Overall values of the C_{31} ββ/(ββ+αβ) hopane ratio range between 0.06 and 0.42, consistent with an acidic peat forming environment. Another unusual feature of these sections is the lack of 6'-methyl brGDGTs in nearly all samples despite reconstructed pH above 5; at such pH and especially above pH 6, 6'-methyl brGDGTs do occur in modern mineral soils and peatlands (Naafs et al. 2018). This is not

497 an artefact of the analytical method, as we cross-checked with the “long” method in Plymouth
498 (Supplementary Fig. S1). Therefore, we interpret our MAAT record cautiously, focusing primarily on
499 the most pronounced variations which are not correlated with changes in CBT. That is, peak
500 temperatures immediately above the K-Pg boundary, and the long-term decline in MAATs in the
501 Paleogene part of the record.

502

503 **Age Model**

504 *Correlation:* First order correlation between the two sites is based on the occurrence of the
505 distinctive Ir-bearing claystone that is also palynologically enriched in fern spores (Sweet and Braman,
506 1992), and marks the base of the Paleogene. Its base is used as a horizontal datum in Figure 2 and
507 Supplementary Figure S2. Jerrett et al. (2015) interpreted these coals to represent, at least in part,
508 small, disconnected rheotrophic mires, readily subject to local autogenic clastic input. Consequently,
509 a lithostratigraphic approach would not be appropriate for the generation of other
510 chronostratigraphic tie-points in this case. Instead, secondary tiepoints are provided by inflexion
511 points on their respective $\delta^{13}C_{org}$ stratigraphies of the two sites (Tiepoints 1–9; Figs. 2 and Supp. Fig.
512 S2). These can be interpreted as representing a more regional stratigraphic signal relating to changes
513 in the carbon isotopic composition of the atmosphere the plants in the peats were metabolising (Arens
514 and Jahren, 2000). This correlation is consistent with an independent correlation between the two
515 sites based on petrographic criteria by Jerrett et al. (2015).

516 *Timescales:* Estimations of the duration of time represented by such short stratigraphies are
517 difficult. Broad estimates of the duration of time represented by the two coal seams, however, can be
518 estimated from the absolute age determinations of Renne et al. (2013) at the coal-bearing K-Pg site at
519 Hell Creek Marina Road (Montana), located 170 km SSW of Rock Creek West (Fig. 1). The stratigraphy
520 of the site is represented by 160 cm of coal, which directly overlies the Ir-enriched claystone marking
521 the K-Pg boundary. The coal contains two tuffs termed Z2 and Z1, 80 cm and 120 cm above the K-Pg

522 boundary, respectively. $^{40}Ar/^{39}Ar$ dating of sanidines in the tuffs yield an age of 66.019 ± 0.021 Ma for
523 Z2, and 66.003 ± 0.033 Ma for Z1 (Renne et al. 2013), giving a most likely duration of 16 ka for the 40
524 cm of intervening coal (i.e., 1 m represents 40 ka). Error estimates of the ages suggest a maximum
525 possible duration of 70 ka is possible for the 40 cm of intervening coal (i.e., 1 m represents 175 ka),
526 and an unlikely minimum duration that equates to instantaneous deposition.

527 In Supplementary Table S3, the most likely (1 m = 40 ka), minimum (1 m = 0 ka), and maximum
528 (1 m = 175 ka) duration of time represented by the coal is used to date Tiepoints 1–9, relative to the
529 K-Pg boundary (Fig. 2 and Fig. S2). Differences in thicknesses of coal between the tiepoints (i.e.,
530 differences in thicknesses of the $\delta^{13}C_{org}$ excursion stratigraphies) at Rock Creek West and Wood
531 Mountain Creek (Fig. 2 and Fig. S2) clearly imply that there were differences in synchronous peat
532 accumulation rates and/or post-depositional compaction of the peat at the two sites (and also
533 between these sites and the Hell Creek Marina Road site of Renne et al. 2013). This highlights
534 uncertainties, but the approach places clear absolute errors in the timescales of MAAT change
535 interpreted in this study. The ages relative to the K-Pg boundary that we use for Tiepoints 1–9 are
536 based on the average determined for Rock Creek West, and Wood Mountain Creek (Supplementary
537 Table S3).

538 Having established the best-estimate ages of Tiepoints 1–9 (Supplementary Table S3), the
539 midpoint of each sample was linearly extrapolated between the ages of the Tiepoints to ascribe each
540 an individual age relative to the K-Pg boundary (Supplementary Table S4). MAAT for each datapoint
541 were plotted against these ages to make Figure 3.

542

543 **FIGURE AND TABLE CAPTIONS**

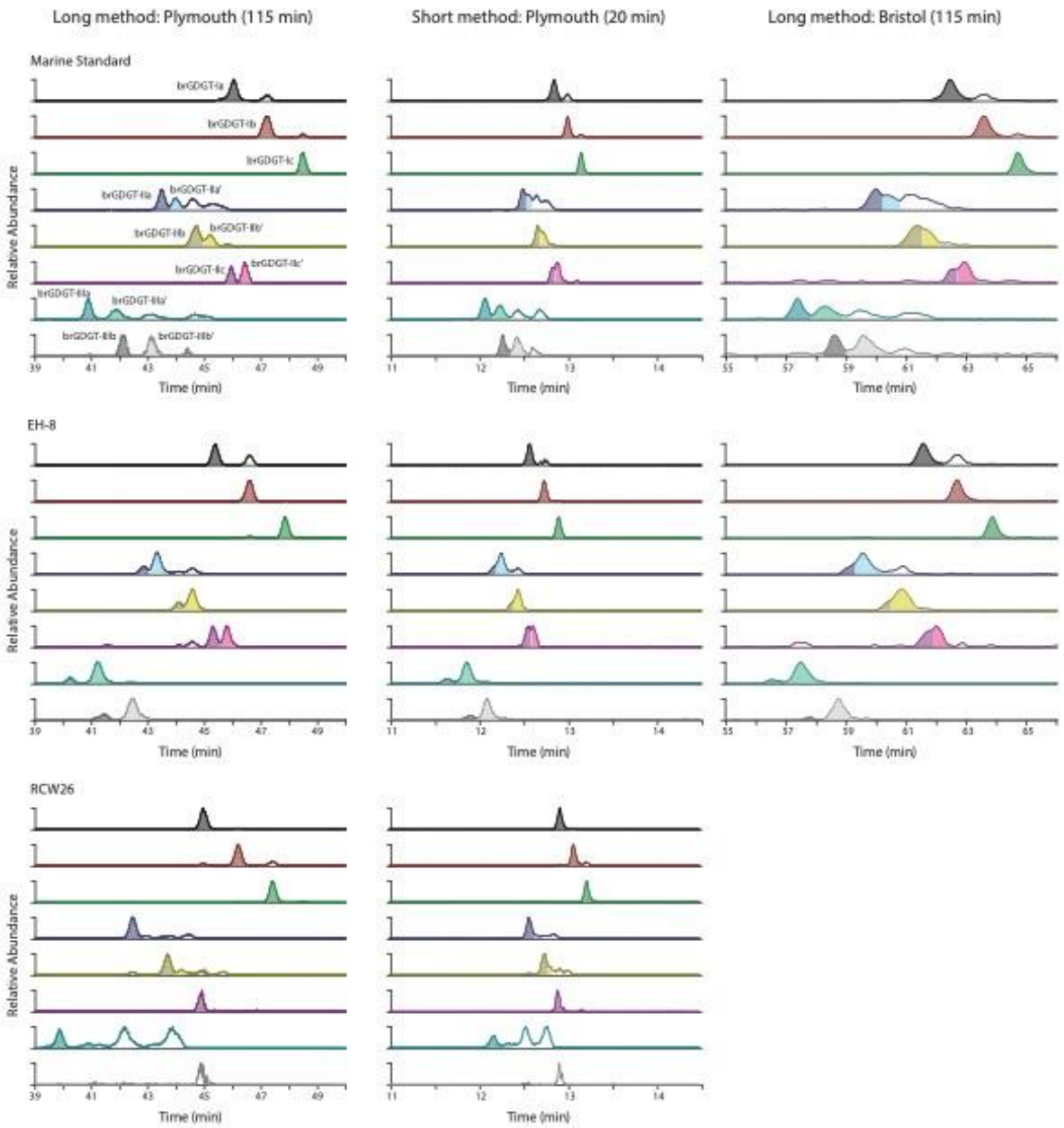

Supplementary figure S1. *Chromatograms showing the difference in resolution of individual brGDGTs and their isomers in the 'Long' method at Plymouth University (A), the 'Short' method at Plymouth University (B), and the 'Long' method at University of Bristol. 6-methyl-GDGTs are indicated with* '.

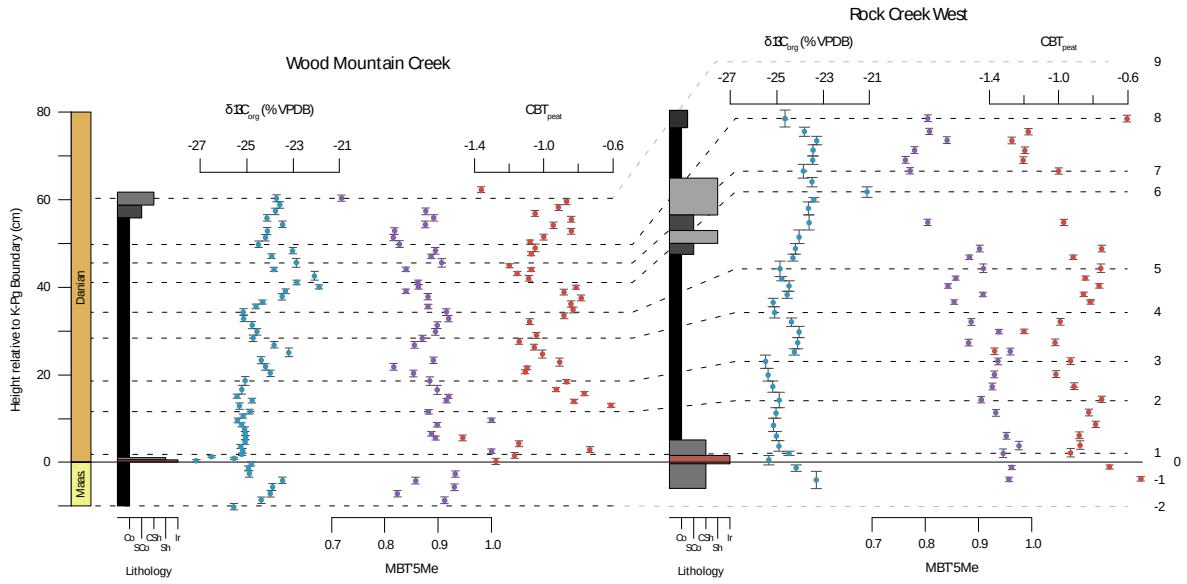

548

549 ***Supplementary figure S2.*** *$\delta^{13}C_{org}$ (blue), brGDGT mean annual air temperature (MAAT; purple), CBT_{peat}-*
550 *pH (red) records from Wood Mountain Creek and Rock Creek West, Saskatchewan, plotted against*
551 *height relative to the K-Pg boundary. Vertical error bars show the stratigraphic range of each sample.*
552 *Dashed lines show chemostratigraphic ($\delta^{13}C_{org}$) correlation tiepoints. Solid line shows the Ir-claystone*
553 *K-Pg datum. On the lithology log, Co = coal, ShC = shaley coal, CSh = coaly shale, Sh = shale, and Ir =*
554 *iridium-enriched claystone.*

555 ***Supplementary Table S1.*** *Stratigraphic and lithological data, GDGT abundances, proxy calculations*
556 *(MBT'5Me, MAAT, CBT, pH, and hopane ratio), and $\delta^{13}C_{org}$ for all samples reported in this study.*
557 *MBT'5Me (Columns X, AO) calculated from De Jonge et al. (2015). MAAT (Columns Y, AP) calculated*
558 *from Naafs et al. (2017). CBTpeat (Columns Z, AQ) calculated from Naafs et al. (2018). pH (Columns*
559 *AA, AR) calculated from Naafs et al. (2018). Hopane ratio (Column AV) calculated from Inglis et al.*
560 *(2018). Blank cells (columns K–W, AB–AN) denote below the detection limit/unquantifiable GDGTs. The*
561 *$\delta^{13}C_{org}$ values (columns AY–BF) for Wood Mountain Creek are from Jerrett et al. (2015). All other data*
562 *was generated for this study. Where the standard deviation of MAAT > 1, this sample was omitted*
563 *from the study. Where polar fraction analysis not undertaken or duplicated, this sample was omitted*
564 *from the study.*

***Supplementary Table S2**. Comparison of MBT, MBT'5Me proxy values calculated from the 'Short' and 'Long' HPLC-APCI-MS methods at Plymouth University and the 'long' method at the University of Bristol. (std= standard, RCW= Rock Creek West, SD= standard deviation).*

***Supplementary Table S3.** Age of Tiepoints 1–9 (Fig. S2) at Rock Creek West and Wood Mountain Creek relative to the K-Pg boundary (columns C–E and G–I respectively), applying the minimum (1 m = 0 ka), most likely (1 m = 40 ka), and maximum (1 m = 175 ka) duration of time represented by the coal from Renne et al. (2013). Also shown are the average relative ages of the tiepoints from Rock Creek West and Wood Mountain Creek (columns L-N). The most likely duration of the average tiepoint ages (column M) are the values used to generate the ages for each datapoint in Supplementary Table S4.*

***Supplementary Table S4.** All samples, and their assigned ages generated through linear interpolation of the position of their midpoint between tiepoints. The ages of the tiepoints are from column M (Supplementary Table S3). Also shown are the MAAT (°C) and mean $\delta^{13}C_{org}$ (‰) values from Supplementary Table S1. These data are used to plot Figure 3.*

***Supplementary Table S5.** Statistical analysis of MAAT data. MAAT data were separated into four temporal bins: pre-K-Pg boundary (-5–0 ka), 0–10 ka, 10–20 ka, and 20–30 ka. These bins were then analysed using two-sample, equal variances t-tests to determine the statistical significance of temperature trends. These data are included in Figure 3.*